Journal of Solid State Electrochemistry (2018) 22:2959–2964
https://doi.org/10.1007/s10008-018-3993-0

ORIGINAL PAPER

Lithium ion conductivity of solid solutions based on Li_8ZrO_6

Mariya S. Shchelkanova[1] · Georgi Sh. Shekhtman[1] · Anastasia V. Kalashnova[1] · Olga G. Reznitskikh[2]

Received: 27 January 2018 / Revised: 17 April 2018 / Accepted: 11 May 2018 / Published online: 22 May 2018

Abstract

Lithium ion conductivity of lithium hexaoxozirconate Li_8ZrO_6 doped by Mg^{2+}, Sr^{2+}, Nb^{5+}, V^{5+}, and Ce^{4+} cations was studied using impedance spectroscopy. The NMR data indicate that in the low-temperature region, lithium ion migration takes place by exchange of Li^+ among tetra- and octahedral positions. Data of Raman spectroscopy suggest that the potential reason for the sharp increase of Li_8ZrO_6 and its solid solutions' conductivity near 700 K may be melting of LiOH which occurs as a result of interaction between samples and atmospheric moisture.

Keywords Solid electrolytes · Lithium ion conductivity · Lithium hexaoxozirconate · Lithium batteries · Raman spectroscopy · Nuclear magnetic resonance

Introduction

Among the electrochemical power sources, one of the leading positions belongs to the lithium-ion batteries (LIBs). Compared with most other kinds of batteries, LIBs have a higher output voltage and higher energy storage density. Of special interest is development of all-solid-state lithium-ion batteries using solid lithium-conducting electrolytes instead of traditional liquid organic or polymer electrolytes. The major advantages of all-solid-state lithium-ion batteries are simple design and, the main thing, safety. According to several works [1], promising solid electrolytes for medium- and low-temperature all-solid-state lithium-ion batteries are LLZ ($Li_7La_3Zr_2O_{12}$, $\sigma_{300\ K} = 2.1 \times 10^{-4}$ S × cm^{-1}) [2], LISICON ($Li_{14}ZnGe_4O_{16}$, $\sigma_{300\ K} = 10^{-7}$ S × cm^{-1}) [3], NASICON-like $Li_{1+x}Al_xTi_{2-x}(PO_4)_3$ ($\sigma_{300\ K} = 7.0 \times 10^{-4}$ S × cm^{-1}) [4], and glass-ceramic $Li_{1.6}Al_{0.6}Ge_{1.4}(PO_4)_3$ ($\sigma_{300\ K} = 4.0 \times 10^{-4}$ S × cm^{-1}) [5]. Unfortunately, most of the above materials have high Li^+ ion conductivity but are unstable in contact with metal lithium. Binary compounds in the system Li_2O-ZrO_2 are free from this disadvantage [6, 7] but their conductivity is too small. Therefore, investigations focused on raising the ionic conductivity of lithium zirconates are of great importance.

Among lithium zirconates, the maximum value of conductivity (10^{-4}–10^{-5} S × cm^{-1} at 570 K) is observed for Li_8ZrO_6 [8, 9].

The first crystal structure and transport properties of Li_8ZrO_6 and Li_7LO_6 (L = Nb, Ta), which have close resemblance, were studied in work [8]. All of these compounds have layered structure derivative of CdI_2. Crystal lattice of both Li_8ZrO_6 and Li_7LO_6 consists of layers containing ions of Zr^{4+} (L^{5+}) and 2 of 8 Li^+ cations in octahedral positions, the remaining 6 Li^+ ions occupy half of tetrahedral sites between layers. Composition of layers may be described as $[(Li_2Zr)O_6]_n$ in case of Li_8ZrO_6 or as $[(Li□L)O_6]_n$ in case of Li_7LO_6. As one can see, Li_7LO_6 compounds contain structural lithium vacancies (□) in octahedral positions; in Li_8ZrO_6 such vacancies are absent. Due to the presence of the lithium vacancies, lithium ion conductivity of Li_7LO_6 is considerably higher as compared to Li_8ZrO_6, which has ordered crystal structure. Therefore, one can expect that the introduction of additives creating vacancies in the lithium sublattice will increase Li^+ ion conductivity of Li_8ZrO_6. Actually, the increase of conductivity is observed at substitution of Li^+ by Mg^{2+} or

Highlights Li_8ZrO_6 doped by M^{2+}, A^{5+}, and Ce^{4+} was studied using impedance, Raman study, and NMR. The maximum conductivity (9×10^{-6} S cm^{-1} at 476 K) is observed for $Li_{7.98}Zr_{0.98}V_{0.02}O_6$. Below 700 K, Li^+ ions move via jumps between octahedral and tetrahedral positions. In all cases, conductivity shows a jump-like rise at 680–710 K. One of the reasons for a jump of conductivity near 700 K may be the melting of LiOH.

✉ Mariya S. Shchelkanova
shchelkanova.mariya@mail.ru

[1] Institute of High-Temperature Electrochemistry, Ural Branch of RAS, Akademicheskaya St., 20, Ekaterinburg 620137, Russian Federation

[2] Institute of Solid State Chemistry, Ural Branch of RAS, GSP, Pervomayskaya St., 91, Yekaterinburg 620990, Russian Federation

Sr^{2+} according to Eq. 1 [10] and at substitution of Zr^{4+} by Nb^{5+} or V^{5+} according to Eq. 2 [11, 12].

$$2Li^{+} \rightarrow Mg(Sr)^{2+} + V_{Li} \quad (1)$$

$$Li^{+} + Zr^{4+} \rightarrow Nb(V)^{5+} + V_{Li} \quad (2)$$

Introduction of additives of another type such as substitution of Zr^{4+} by triple-charged cations Al^{3+}, Y^{3+}, and Sc^{3+} with charge compensation by interstitial Li^{+} ions is not followed by conductivity rise [13–15]. It is of interest that a considerable increase of conductivity takes place at isovalent substitution of Zr^{4+} by Ce^{4+} [16].

In this paper, the values of conductivity in the solid solutions $Li_{8-2x}Me_xZrO_6$ (Me = Mg, Sr), $Li_{8-x}Zr_{1-x}A_xO_6$ (A = V, Nb), and $Li_8Zr_{1-x}Ce_xO_6$ are compared, and temperature dependences of conductivity of these solid solutions are analyzed. A number of samples were examined by Raman spectroscopy and nuclear magnetic resonance (NMR) spectroscopy. Based on the data obtained, conclusions about factors determining high conductivity of the materials under consideration are made.

Experimental

According to work [11], the range of solid solutions based on Li_8ZrO_6 in the system $Li_{8-x}Zr_{1-x}V_xO_6$ lies at $x < 0.05$. The data of the present study show that single-phase region boundary in this system corresponds to $x \approx 0.02$. Furthermore, $Li_{7.98}Zr_{0.98}V_{0.02}O_6$ solid solution has the highest conductivity in $Li_{8-x}Zr_{1-x}V_xO_6$ system. So, to compare the values of conductivity in other systems with heterovalent substitutions, we chose compositions with the same value $x = 0.02$, that is, with the equal concentration of lithium vacancies: $Li_{7.96}\square_{0.02}Me_{0.02}ZrO_6$ (Me = Mg, Sr) and $Li_{7.98}\square_{0.02}Zr_{0.98}A_{0.02}O_6$ (A = V, Nb). All these compositions lie in the single-phase regions of the corresponding systems and have conductivity close to maximal value. A sample containing niobium was synthesized and studied in this work. The data on conductivity of Mg- and Sr-containing solid solutions are taken from several works [17, 18]. In the system $Li_8Zr_{1-x}Ce_xO_6$ as well as in the systems with heterovalent dopants, a sample with $x = 0.02$ was studied.

Li_2CO_3 (high purity) and V_2O_5, Nb_2O_5, CeO_2, and ZrO_2 (analytical grade) were used as starting materials for the solid-state synthesis of $Li_8Zr_{0.98}Ce_{0.02}O_6$, $L_{7.98}Zr_{0.98}Nb_{0.02}O_6$, and $Li_{7.98}Zr_{0.98}V_{0.02}O_6$. Zirconium, niobium, and cerium oxides were pre-dried at 1270 K to a constant weight. The starting materials were mixed in a stoichiometric ratio, except for Li_2CO_3, which was added with 5–8 wt% surplus. The syntheses were carried out in glass carbon crucibles under vacuum in the hermetic heatproof steel reactor. The synthesis was carried out by stepwise increasing the temperature from 573 to 1253 K. Then, the samples were annealed in the air at 873 K for 6 h to remove traces of carbon.

The crystal structure of the products obtained was determined by the X-ray diffraction (XRD) after each stage of the synthesis. The XRD analysis was carried out using Rigaku D-MAX-2200 V diffractometer in CuKα-radiation, $2\theta = 10°–80°$. XRD patterns of compounds were compared with database PDF-2 [19] and literature data.

Chemical analysis of synthesized samples was performed using inductively coupled plasma atomic emission spectrometer OPTIMA 4300 DV (Perkin Elmer, USA).

Raman spectra of the polycrystalline samples were collected with Raman microscope-spectrometer RENISHAW U-1000 (Ar^{+}-radiation, $\lambda = 514$ nm) at 50–4000 cm^{-1}.

Thermal analysis of the materials obtained was performed using synchronous thermal analyzer STA 449 F1 Jupiter over the temperature range 300–870 K in alundum crucibles at the rate of heating 10 K min^{-1} in the air. The mass of the samples was 10–20 mg. The data obtained were processed by means of NETZSCH Proteus software.

NMR experiments were carried out using an updated Bruker SXP 4-100 pulsed NMR spectrometer at resonance frequency 194.37 MHz in the temperature range 300–670 K. NMR spectra and the spin-lattice relaxation time of ^7Li nuclei were measured by the Fourier transformation of the signal of the free induction decay.

The samples for conductivity measuring with diameter 6 mm and thickness 1–2 mm were obtained by pressing the powders of particle size < 50 μm in the steel die at 70 MPa. Then the samples were covered by the powder of the same composition and sintered under helium in the heatproof steel reactor for 5 h at 1179 K. The density of the samples calculated from the geometrical parameters and mass was 90–95% of the theoretical one.

For AC impedance studies, both sides of the sintered samples were painted with silver paste. The impedance measurements were performed in the air at temperatures ranging from 25 to 600 °C, using an immittance meter E7-25 (MNIPI) in the frequency range from 20 Hz to 1 MHz. The results were fitted by using special software program (EQUIVCRT.COM). All of the conductivity measurements were performed on two sets of identical samples to check the reproducibility of the results.

Electron conductivity was measured at direct current using blocking Ag [15] electrodes in the temperature range 470 to 870 K. For this purpose, direct voltage which was less than solid electrolyte decomposition voltage (20–40 mV) was applied to Ag | solid electrolyte | Ag cell. After a time, the current acquired a fixed value. Under these conditions, ionic current is blocked and the charge is carried by electrons and holes. Knowing the current value and applied voltage, we can calculate the electron conductivity.

Results and discussion

Ionic conductivity and DSC

Figure 1 shows XRD patterns of the samples studied. It is seen that in all cases, diffraction diagram corresponds to the Li_8ZrO_6 phase (PDF2 No. 26-0867 card-index data).

Temperature dependences of conductivity for Li_8ZrO_6 and solid solutions are similar (Fig. 2). Low- and high-temperature linear regions are separated at 680–710 K by a transition section, which is characterized by a sharp increase in conductivity with increasing temperature. Electron conductivity value of both undoped Li_8ZrO_6 and solid solutions in all cases was by three orders of magnitude less than ionic one. Therefore, further on when discussing the synthesized material conductivity, we mean their ionic conductivity. DSC measurements of Li_8ZrO_6 show the existence of endothermic peak at 680 K (Fig. 3). The enthalpy of effect is − 23.6 J g^{-1}. DSC curves of the doped samples also show endothermic peaks in the range 680–700 K. In all cases, the temperature of thermal effect is close to the temperature of the drastic change in conductivity. It gives reason to suggest that at 680–710 K, the materials examined undergo a phase transition followed by lithium sublattice disorder [10]. However, there is another probable interpretation of Li_8ZrO_6 and its solid solutions' conductivity behavior. The fact is that binary compounds of the Li_2O–M_xO_y systems with the high content of lithium oxide, such as Li_5MO_4 (M = Al, Ga [20], Fe [21], Tl [22]), Li_6ZnO_4 [20], Li_7LO_6 (L = Bi, Sb, Ta) [23], and also Li_8ZrO_6 [24], are highly hygroscopic and interact with ambient air moisture. For the first time, influence of this effect on conductivity was found for Li_5AlO_4. The first conductivity measurements of Li_5AlO_4 as well as of Li_5GaO_4 and Li_6ZnO_4 showed [20] that at

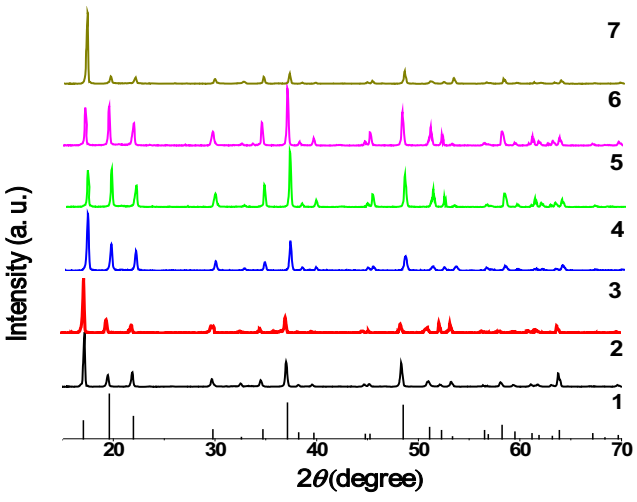

Fig. 1 XRD patterns of (1) Li_8ZrO_6 PDF2 # 26-0867 and (2) undoped Li_8ZrO_6 phase and (3) $Li_{7.98}Zr_{0.98}V_{0.02}O_6$, (4) $Li_{7.98}Zr_{0.98}Nb_{0.02}O_6$, (5) $Li_8Zr_{0.98}Ce_{0.02}O_6$, (6) $Li_{7.96}Sr_{0.02}ZrO_6$, and (7) $Li_{7.96}Mg_{0.02}ZrO_6$ solid solutions

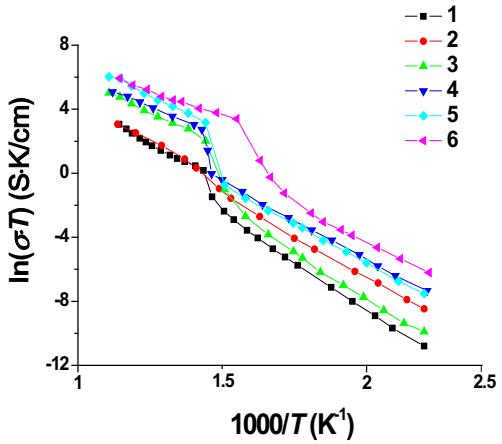

Fig. 2 Arrhenius plots for (1) Li_8ZrO_6 and (2) $Li_8Zr_{0.98}Ce_{0.02}O_6$, and (3) $Li_{7.96}Sr_{0.02}ZrO_6$, (4) $Li_{7.98}Zr_{0.98}Nb_{0.02}O_6$, (5) $Li_{7.96}Mg_{0.02}ZrO_6$, and (6) $Li_{7.98}Zr_{0.98}V_{0.02}O_6$ solid solutions

heating up to ~ 680 K, the conductivity of these materials increases jump-like achieving 10^{-1} S × cm^{-1} but activation energy decreases sharply. At first, such a behavior as in the case of Li_8ZrO_6 was explained by lithium sublattice disorder [23]. However, later, it was shown through the example of Li_5AlO_4 that the jump-like increase of conductivity in this case is due to the melting of LiOH, which appears as a result of interaction between Li_5AlO_4 and atmospheric moisture [25, 26]. If one compares temperature dependences of conductivity for Li_5AlO_4, Li_5FeO_4, Li_5TlO_4, Li_8ZrO_6, and its solid solutions (Fig. 2) and Li_7LO_6 (L = Bi, Sb, Ta) [23], it can readily be seen that in all cases, $\lg\sigma - 1/T$ curves demonstrate the same peculiarities. First, one observes a sharp increase in conductivity and decrease in activation energy, and this at similar temperatures which are close to the melting point of LiOH (680–710 K). Second, in all cases, DTA or DSC measurements indicate an endothermic peak in the same temperature region. Third, the presence of a jump in conductivity and its temperature does not depend on introduction of additives,

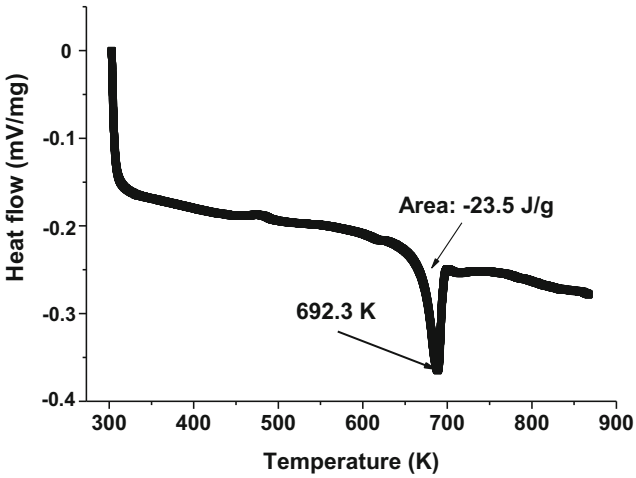

Fig. 3 DSC plot of Li_8ZrO_6: heating rate 10 K min^{-1}

their nature, and concentration. The assumption about the absence of phase transition in Li_8ZrO_6 near 700 K is supported by the fact that high-temperature XRD study does not show a change of the crystal structure, which was to be expected at disorder of cation sublattice. The X-ray pattern obtained at 893 K [27] is identical to that obtained at room temperature [28].

Raman spectroscopy

Table 1 shows the observed bands of the Raman spectra for Li_8ZrO_6 and some of the solid solutions synthesized in this work as compared to the literature data. One can see that the spectra of Li_8ZrO_6 and its solid solutions contain a number of extra bands, which were not observed for Li_8ZrO_6 in work [23]. However, most of these extra bands may be referred to Li_2CO_3, LiOH, and $LiOH{\cdot}H_2O$ [29–31]. The formation of LiOH as a result of interaction between Li_8ZrO_6 and water vapor according to the reaction

$$Li_8ZrO_6 + 2H_2O \rightarrow Li_4ZrO_4 + 4LiOH \quad (3)$$

was experimentally proved in work [24]. It seems that the formation of $LiOH{\cdot}H_2O$ and Li_2CO_3 is a result of the further interaction of LiOH and atmosphere moisture and CO_2. Therefore, it is reasonable to assume that the anomalous behavior of conductivity of Li_8ZrO_6 and its solid solutions may be due to the formation of LiOH, which melts at elevated temperatures as in the case of Li_5AlO_4. As concerns Li_7LO_6 (L = Nb, Ta, Sb, Bi), the authors [23] do not find in the samples studied any interaction with atmosphere products, but do not register any change in crystal lattice at temperatures above 700 K either. Therefore, the point of sharp increase in conductivity of the materials under discussion when heated to ~ 700 K remains unclear.

NMR spectroscopy

^{7}Li NMR experiments were performed for $Li_{7.98}Zr_{0.98}V_{0.02}O_6$ solid solution in the temperature range 300–750 K (Fig. 4).

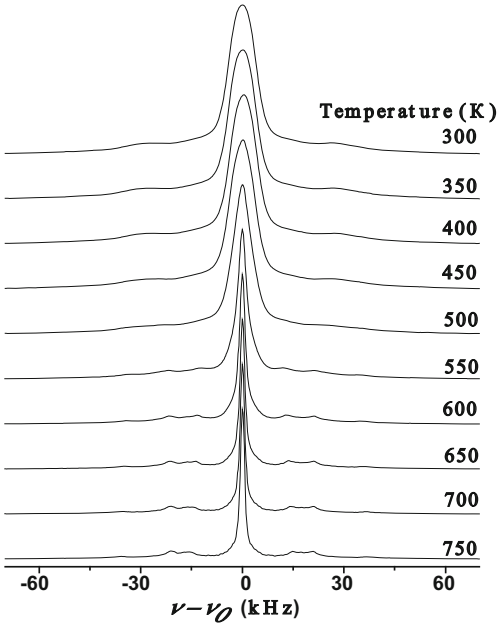

Fig. 4 ^{7}Li NMR spectra as a function of temperature for $Li_{7.98}Zr_{0.98}V_{0.02}O_6$

Modeling of the spectrum shape shows that spectral line can be described as superposition of two lines which correspond to different structural positions of lithium Li1 and Li2. Such positions in solid solutions with Li_8ZrO_6 structure are represented by octahedral positions in layers and tetrahedral ones between layers. ^{7}Li NMR spectra for undoped Li_8ZrO_6 are similar [9].

Figure 5 shows ^{7}Li NMR line width of the central transition as function of temperature. As one can see, at temperature increase, the width of ^{7}Li NMR line is gradually reduced. Such behavior of NMR spectra is typical for systems with fast ion transport. Sharp narrowing of NMR line takes place when characteristic frequency of diffusion τ_d^{-1} approaches the width of the NMR line of rigid lattice. For $Li_{7.98}Zr_{0.98}V_{0.02}O_6$ solid solution, this temperature area is ~ 450–600 K (Fig. 5). Earlier, close temperature interval of NMR line narrowing was observed for undoped Li_8ZrO_6 [9]. It should be pointed out that for Li_7LO_6, which has a similar crystal structure but contains

Table 1 Observed absorption bands (cm^{-1}) in the Raman spectra for Li_8ZrO_6 and solid solutions $Li_{7.98}Zr_{0.98}V_{0.02}O_6$, $Li_{7.98}Zr_{0.98}Nb_{0.02}O_6$, and $Li_8Zr_{0.98}Ce_{0.02}O_6$ as compared to literature data

Band positions (cm^{-1})	Band assignments	Ref.
202, 273, 414, 462, 526, 618, 668	Li_8ZrO_6	23
96, 155, 193, 298, 417, 463, 573, 628, 672	Li_8ZrO_6	
96, 118, 155, 201, 242, 275, 294, 330, 416, 464, 520, 620, 670	$Li_{7.98}Zr_{0.98}Nb_{0.02}O_6$	
96, 126, 156, 193, 238, 274, 301, 373, 414, 457, 507, 569,634, 708	$Li_{7.98}Zr_{0.98}V_{0.02}O_6$	
96, 155, 194, 275, 415, 453, 519, 560, 630, 705	$Li_8Zr_{0.08}Ce_{0.02}O_6$	
97, 128, 157, 194, 274, 380, 518, 714	Li_2CO_3	29
		30
299, 329, 519, 620	LiOH	31
117, 249, 369, 413, 524, 632, 672	$LiOH{\cdot}H_2O$	29

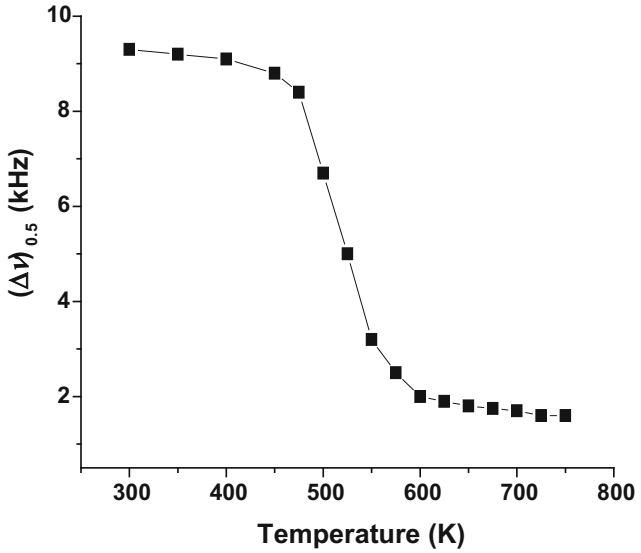

Fig. 5 ^{7}Li NMR line width (full width at half-height) as a function of temperature for $Li_{7.98}Zr_{0.98}V_{0.02}O_6$

structural lithium vacancies close to ^{7}LiNMR, the line is observed at essentially lower temperatures 200–400 K [23], which correlates with higher Li^+ conductivity of Li_7LO_6 as compared to Li_8ZrO_6.

Activation energy for jumps of Li^+ ions in solid solution $Li_{7.98}Zr_{0.98}V_{0.02}O_6$ calculated from NMR data at low temperatures is equal to 44 kJ × mol^{-1}, whereas the value obtained from the temperature dependence of conductivity is more than twice as large (99 kJ × mol^{-1}). It suggests that the total mobility of lithium is to a great degree due to the local jumps of Li^+.

The results of the transport property study of materials under discussion are summarized in Table 2. One can see that introduction of dopants in all cases results in conductivity increase and activation energy lowering as compared to undoped Li_8ZrO_6. In case of systems with two- and fifth-charged dopants, it is due to formation of lithium vacancies. Unlike Li_7LO_6, charge carriers in Li_8ZrO_6 are thermal activated defects rather than structural vacancies. At substitution of Li^+ or Zr^{4+} ions by M^{2+} or A^{5+} ions respectively, the concentration of lithium vacancies drastically increases but activation energy decreases by a value of defect formation. Both factors lead to the increase of conductivity. The growth of conductivity at isovalent substitution of Zr^{4+} by Ce^{4+} seems to be a result of geometrical changes. As ion radius of Ce^{4+} is essentially larger compared to Zr^{4+} (0.87 and 0.76 Å respectively) [32], the substitution of Ce^{4+} for Zr^{4+} should lead to broadening of lithium migration channels and lowering of the average value of potential barrier which separates an occupied Li^+ position in the crystal lattice from a vacant one.

Table 2 Ionic conductivities and the activation energies for Li_8ZrO_6 and solid solutions $Li_{7.98}Zr_{0.98}A_{0.02}O_6$ (A = V, Nb), $Li_{7.96}Me_{0.02}ZrO_6$ (Me = Mg, Sr), and $Li_8Zr_{1-x}Ce_xO_6$

Compound	σ (S × cm^{-1})		E_a (kJ × mol^{-1})	
	833 K	454 K	Temperature region	
			High	Low
Li_8ZrO_6	8.7×10^{-3}	4.8×10^{-8}	76	99
$Li_{7.98}Zr_{0.98}Nb_{0.02}O_6$	1.0×10^{-1}	1.5×10^{-6}	53	80
$Li_{7.98}Zr_{0.98}V_{0.02}O_6$	2.5×10^{-1}	4.6×10^{-6}	50	75
$Li_8Zr_{0.98}Ce_{0.02}O_6$	1.3×10^{-2}	5.2×10^{-7}	74	88
$Li_{7.96}Mg_{0.02}ZrO_6$	2.3×10^{-1}	1.2×10^{-6}	65	85
$Li_{7.96}Sr_{0.02}ZrO_6$	6.3×10^{-2}	1.2×10^{-7}	70	95

It should be noted, however, that conductivity increase of Li_8ZrO_6 at introduction of dopants in low-temperature region in all cases is not very large. Maximal value of conductivity is observed for $Li_{7.98}Zr_{0.98}V_{0.02}O_6$ and is equal to $8.9 \cdot 10^{-6}$ S × cm^{-1} at 476 K (Table 2). That is only six times as large as compared to undoped Li_8ZrO_6. Rather low value of conductivity is the result of low solubility of the dopants and, as a consequence, low concentration of lithium vacancies. In Li_7LO_6, half of the octahedral Li^+ positions are vacant, so its lithium ion conductivity is essentially higher and for Li_7BiO_6 achieves 3×10^{-3} S × cm^{-1} at 476 K [23].

In the high-temperature region, the conductivity of Li_8ZrO_6 and solid solutions based on it drastically increases and at 870 K achieves 10^{-1} S × cm^{-1} (Table 2). However, the reasons for such a behavior are not well established. A possible solution to this problem could be a precise neutron diffraction study of crystal structure in the temperature region of existence of supposed disordered form of Li_8ZrO_6 or an investigation into the dependence of conductivity as function of time at ~ 800 K at a change of dry atmosphere into moisture and vice versa as it was done in [33].

Conclusion

Temperature dependences of conductivity and Raman spectra of solid solutions based on lithium hexaoxozirconate $Li_{7.96}Me_{0.02}ZrO_6$ (Me = Mg, Sr), $Li_{7.98}Zr_{0.98}A_{0.02}O_6$ (A = V, Nb), and $Li_{7.98}Zr_{0.98}Ce_{0.02}O_6$ are investigated. Ionic conductivity at doping increases as compared to Li_8ZrO_6; however, below ~ 680 K, it remains rather low and significantly smaller as compared to Li_7LO_6 (L = Nb, Ta, Sb, Bi), which have the similar crystal structure but contain structural lithium vacancies.

Conductivity of both undoped Li_8ZrO_6 and solid solutions shows a jump-like rise with increasing temperature at 680–710 K. Earlier, such a behavior was explained by a structural phase transition with disordering of the lithium sublattice. The data of Raman spectroscopy, however, shows that the melting of lithium hydroxide formed due to interaction of samples

with atmospheric moisture may be another reason for a sharp growth of conductivity near 700 K.

The results of NMR experiments show that at low temperatures, the movement of lithium cations in the crystal lattice takes place via exchange between octahedral and tetrahedral positions.

Acknowledgments The authors are grateful to S.V. Plaksin and E.G. Vovkotrub. The research has been carried out with the equipment of the Shared Access Center "Composition of Compounds" of the Institute of High-Temperature Electrochemistry of Ural Branch of RAS, Yekaterinburg, Russian Federation.

References

1. Cao C, Li ZB, Wang XL, Zhao XB, Han WQ (2014) Recent advances in inorganic solid electrolytes for lithium batteries. Front Energy Res 2. https://doi.org/10.3389/fenrg.2014.00025
2. Dumon A, Huang M, Shen Y, Nan CW (2013) High Li ion conductivity in strontium doped $Li_7La_3Zr_2O_{12}$ garnet. Solid State Ionics 243:36–41
3. Hong HY-P (1978) Crystal structure and ionic conductivity of $Li_{14}Zn(GeO_4)_4$ and other new Li^+ superionic conductors. Mater Res Bull 13(2):117–124
4. Aono H, Sugimoto E, Sadaoka Y, Imanaka N, Adachi G (1990) Ionic conductivity of solid electrolytes based on lithium titanium phosphate. J Electrochem Soc 137(4):1023–1027
5. Fu J (1997) Fast Li^+ ion conducting glass-ceramics in the system Li_2O–Al_2O_3–GeO_2–P_2O_5. Solid State Ionics 104(3-4):191–194
6. Hellstrom EE, Gool van W (1981) Li ion conduction in Li_2ZrO_3, Li_4ZrO_4, and $LiScO_2$. Solid State Ionics 2(1):59–64
7. Moiseev GK, Vatolin NA (2003) Interaction of lithium zirconate with lithium under equilibrium conditions. Dokl Phys Chem 388(4/6):33–37
8. Delmas C, Maazaz A, Guillen F, Fouassier C, Reau JM, Hagenmuller P (1979) Des conducteurs ioniques pseudo-bidimensionnels: Li_8MO_6 (M = Zr, Sn), Li_7LO_6 (L = Nb, Ta) et $Li_6In_20_6$. Mat Res Bull 14(5):619–625
9. Pantyukhina MI, Shchelkanova MS, Stepanov AP, Buzlukov AL (2010) Investigation of ion transport in Li_8ZrO_6 and $Li_6Zr_2O_7$ solid electrolytes. Bull Russ Acad Sci: Phys 74(5):653–655
10. Shchelkanova MS, Pantyukhina MI, Kalashnova AV, Plaksin SV (2016) Electrochemical properties of $Li_{8-2x}M_xZrO_6$ (M = Mg, Sr) solid electrolytes. Solid State Ionics 290:12–17
11. Shchelkanova MS, Pantyukhina MI, Antonov BD, Kalashnova AV (2014) Produce new solid electrolytes based on the Li8-xZr1-xVxO6. Butlerov Commun (in Russian) 38:96–102
12. Pantyukhina MI, Shchelkanova MS, Plaksin SV (2013) Synthesis and electrochemical properties of $Li_{8-x}Zr_{1-x}Nb_xO_6$ solid solutions. Phys Solid State 55(4):707–709
13. Andreev OL, Pantyukhina MI, Martem'yanova ZS, Batalov NN (2003) Ionic conductivity and thermodynamic properties of solid electrolytes based on lithium orthozirconate. Electrochemical Energetic 3:86–90 (in Russian)
14. Pantyukhina MI, Andreev OL, Martem'yanova ZS, Batalov NN (2004) Cation conductivity of Li_8ZrO_6–$LiYO_2$ solid solutions. Inorg Mater 40(4):404–406
15. Huang S, Fang Y, Wang B, Wilson BE, Tran N, Truhlar DG, Stein A (2016) Conduction and surface effects in cathode materials: Li_8ZrO_6 and doped Li_8ZrO_6. J Phys Chem C 120(18):9637–9649
16. Pantyukhina MI, Shchelkanova MS, Plaksin SV (2013) Electrochemical properties of solid solutions in the $Li_8Zr_{1-x}Ce_xO_6$ system. Russ J Electrochem 49(2):144–148
17. Pantyukhina MI, Shchelkanova MS, Plaksin SV (2010) Ionic conduction of $Li_{8-2x}Mg_xZrO_6$ solid solutions. Russ J Electrochem 46:831–834
18. Pantyukhina MI, Shchelkanova MS, Plaksin SV (2012) Ionic conductivity of $Li_{8-2x}Sr_xZrO_6$. Inorg Mater 48(4):382–385
19. PDF2 (JCPDS-ICCD) (Joint committee of powder diffraction standards)
20. Raistrick ID, Ho C, Huggins AR (1976) Lithium ion conduction in $LiAlO_4$, Li_5GaO_4, and Li_6ZnO_4. Mater Res Bull 11(8):953–958
21. Ramdani A, Brice JF (1981) Etude des proprietes de conduction electrique du Ferrite Li_5FeO_4. Ann Chim 6:569–578
22. Nagano N, Greenblatt M (1987) Structural and electrical properties of Li_5TlO_4. Solid State Ionics 24(2):169–174
23. Muhle C, Dinnebier RE, van Wullen L, Schwering G, Jansen M (2004) New insights into the structural and dynamical features of lithium hexaoxometalates Li_7MO_6 (M = Nb, Ta, Sb, Bi). Inorg Chem 43(3):874–881
24. Ohno H, Konishi S, Nagasaki T, Kurasawa T, Katsuta H, Watanabe H (1985) Electrical conductivity of a sintered pellet of octalithium zirconate. J Nucl Mat 132(3):222–230
25. Biefeld RM, Johnson RT (1979) The effects of Li_2SO_4 addition, moisture, and LiOH on the ionic conductivity of Li_5AIO_4. J Solid State Chem 29(3):393–399
26. Johnson RT, Biefeld RM (1979) Ionic conductivity of Li_5AlO_4 and Li_5GaO_4 in moist air environments: potential humidity sensors. Mat. Res. Bull. 14(4):537–542
27. Pantyukhina MI, Andreev OL, Antonov BD, Batalov NN (2002) Synthesis and electrical properties of lithium zirconates. Russ J Inorg Chem 47:1630–1633
28. Scholder R, Räde D, Schwarz H (1968) Uber Zirkonate, Hafnate und Thorate von Barium, Strontium, Lithium und Natrium. Z Anorg Allg Chem Bd 362(3-4):149–168
29. Charton S, Maupoix C, Delaunay F, Saviot L, Bernard F (2016) Experimental investigation on lithium hydride hydrolysis. Thesis, Lyon (France), WHEC16
30. Brooker MH, Bates JB (1971) Raman and infrared spectral studies of anhydrous Li_2CO_3 and Na_2CO_3. J Chem Phys 54(11):4788–4791
31. Harbach F, Ficher F (1975) Raman spectra of lithium hydroxide single crystals. J Phys Cha Solids 36:60l–603l
32. Shannon RD (1976) Revised effective ionic radii and systematic studies of interatomic distances in halides and chalcogenides. Acta Cryst A32:751–767
33. Johnson RT, Biefeld RM, Keck JD (1977) Ionic conductivity in Li_5AlO_4 and LiOH. Mat Res Bull 12(6):577–587